Mechanism and Machine Theory 98 (2016) 164–179

Contents lists available at ScienceDirect

Mechanism and Machine Theory

journal homepage: www.elsevier.com/locate/mechmt

Optimal design under uncertainty of bearing arrangements

Lucian Tudose, Florina Rusu *, Cristina Tudose

Technical University of Cluj-Napoca, Faculty of Machine Building, Department of Mechanical System Engineering, Bvd. Muncii 103-105, 400641 Cluj-Napoca, Romania

ARTICLE INFO

Article history:
Received 9 January 2015
Received in revised form 14 September 2015
Accepted 18 December 2015

Keywords:
Optimal design
Bearing loads
Slope-deflection method
Angular contact ball bearings
Uncertainty
Stochastic optimization

ABSTRACT

This study presents a methodology for an optimal design under uncertainty of a real bearing arrangement. The aim is to find the optimal bench bearing arrangement preload/clearance that maximizes the life of the bearing arrangement considering several uncertain geometric and operating parameters. The paper also presents a new systemic method used to determine the bearing loads required for the life calculations of the bearing arrangements. This method is suitable to be used within an Evolutionary Algorithm due to the fact that it is fast and reliable. The optimal design of the considered bearing arrangement—from the maximum bearing life standpoint—is achieved using a new and efficient stochastic optimization tool obtained by combining the features of Cuckoo Search algorithm and the ones of the Knowledge Gradient policy. Also, a specific approach for optimization under uncertainty using three stages is proposed in this paper. The obtained results are validated by Monte Carlo Sampling.

1. Introduction

Production of large amounts of bearing arrangements destined to work in different applications requires a special management than unique assemblies with the mating parts already measured and the working temperature very precisely estimated or known. For the latter any company can offer reliable information regarding the life of the bearing arrangement, but for the former it is almost impossible to make an accurate prediction without a powerful tool.

The bearing arrangement considered for optimization in this study is a particular one from the first category. Considering that the purpose is to find the optimal design that maximizes the bearing arrangement life based on the value of the bench bearing arrangement preload/clearance an optimization tool and one or more objective functions (based on reliable but fast models) and constraints have to be used in the early phase of the design. Even if it might seem as a simple problem at first glance, it is actually quite complicated because the lifetime calculation requires the real compressive forces that act on the rolling elements of the bearings to be known. These forces depend on the loads transmitted from the shaft to the bearings and therefore, a simple, reliable, but fast model has to be used for bearing load calculation within the optimization tool.

The Finite Element Analysis (FEA) is not a viable option due to the extremely long necessary running time. Even conducting an optimization with an accelerated Evolutionary Algorithm (EA) the order of magnitude of the number of the objective function calls is of hundreds of thousands and therefore, other model than FEA has to be used. Furthermore, the early phase of the design is governed by uncertainty. Even though the tolerances are known, the exact values of the interference between the shaft and the bearing inner ring bore and of the clearance between the housing bore and the bearing outer ring are unknown. Also, the working temperature cannot be rigorously identified, it can only be estimated. Considering the abovementioned aspects, the need for an efficient optimization tool, a fast model to substitute FEA, and a specific approach to deal with uncertainty is indisputable.

* Corresponding author. Tel.: +40 746035549.
E-mail addresses: Lucian.Tudose@omt.utcluj.ro (L. Tudose), Florina.Rusu@omt.utcluj.ro (F. Rusu), Cristina.Stanescu@omt.utcluj.ro (C. Tudose).

http://dx.doi.org/10.1016/j.mechmachtheory.2015.12.008
0094-114X/

Optimizations under uncertainty have been conducted in other fields or subfields such as portfolio management [1], option pricing [2], medicine [3], mining sector [4], chemistry [5], logistics [6], and engineering [7]. In another train of thoughts many scientific papers deal with the optimization of different machine elements, but there is a small number of available papers focused on the optimization of the rolling bearings. Charabotry [8] describes a mono-objective optimization of a ball bearing having five design variables using genetic algorithms. The aim was the maximization of the fatigue life. Rao and Tiwari [9] presented an optimal design methodology of ball bearings based on the maximization of the lifetime. The mono-objective optimization was also conducted using genetic algorithms. A multi-objective optimization with non-conflicting objectives was conducted using NSGA II (non-dominated sorting based genetic algorithm) [10]. Another multi-objective optimization with two objective functions (the basic dynamic radial load rating of the bearing and the minimum thickness of the elastohydrodynamic film between rollers and raceways) was performed using a multi-objective EA in order to obtain the optimal design of a single-row cylindrical roller bearing [11]. However, none of the papers presents an optimization under uncertainty, despite the fact that a high degree of uncertainty could be associated with the design and manufacturing of rolling bearing arrangements.

2. Research background

2.1. Bearing load models

After Sjoväll's pioneering work [12], probably the first general equations for the elastic equilibrium of a ball bearing in three of the five possible degrees of freedom were given by Jones in 1946 [13]. Several years later he has brilliantly completed his work [14] and a general model was issued, whereby the elastic compliances of a system of any number of ball and radial roller bearings under any system of loads can be determined. The system approach signifies that the entire assemblage of bearings, shaft, and supporting structure was looked at as a single, elastic system. The solution defines the elastic compliance of a point on the shaft with respect to the supporting structure in five degrees of freedom. Considering also the centrifugal forces and gyroscopic moments acting on the rolling elements, the internal load distribution is determined for all of the bearings in the system. Finally, bearing lives are evaluated by summation of the fatigue effects of the passages of the rolling elements over precisely determined paths in each bearing raceway.

In a two-part work, De Mul et al. constructed a general mathematical model for the calculation of the equilibrium and associated load distribution in both ball [15] and roller bearings [16]. The bearings may be loaded—with known loads and moments—and displaced in five degrees of freedom. The analysis is made with and without taking into account the centrifugal forces acting on the rolling elements, whilst the internal friction is neglected.

In order to derive a bearing stiffness model for vibration transmission analysis Lim and Singh [17] had to establish the relationships between the known bearing loads and moments transmitted through the rolling element bearing and the bearing displacements in 5 DOF. The reader could find more details in the authors' previous work [18]. In 2012, Gunduz [19] continued this work and developed the formulation of the stiffness matrix for a double-row angular ball bearing.

Houpert [20] proposed a so-called *uniform analytical approach* for ball and roller bearings which provides simple analytical equations to calculate the bearing loading (three loads and two tilting moments) based on the bearing raceway relative displacements (5 DOF). The interesting component of this approach is the manner of introducing the so-called *equivalent displacements* and expressing the rolling element-race load as a function of them. Moreover, the three components of the load and the two components of the moment on the inner raceway are calculated by integration, not by discrete summation. In 2014, Houpert strongly enhanced his model [21], especially for roller bearings.

Hernot et al. [22] presented two stiffness matrices of angular contact ball bearings. Using the two leading Sjoväll's load-distribution integrals J_a and J_r, the summation of ball-raceway loads was replaced by an integration and, in this way, the matrix connected to the conventional model in 2 DOF is first introduced. Using the constructed model, a study of a two bearing-shaft assembly where shaft deformations are ignored, was carried out. But, by taking preload into account it was clearly demonstrated how the influence of the preload on the assembly rigidity and bearing fatigue life may be analyzed. Conclusively, the matrix formulation of the 5 DOF model, connected with the Houpert's early model [20], is presented.

In two successive papers, Liao and Lin first established [23] and then developed [24] a tree-dimensional expression for the elastic deformation of bearing balls in terms of the geometry of the contact surface and the inner and outer raceway positions. Bai and Xu [25] reported a dynamic model of ball bearings used to study the dynamic properties of a rotor system supported by ball bearings under the effect of both internal clearance and raceway waviness. The proposed model includes centrifugal forces and gyroscopic moments.

Relative to our preeminent topic, in the fundamental two-volume monograph, Harris and Kotzalas presented either the Sjoväll's model of load distribution within ball and roller bearings under given external radial and axial load [26], or, partially [27], the Jones' already mentioned work.

Recent works are focused on obtaining the bearing stiffness matrix by extending the Jones' approach as Noel et al. [28] or by using FEM as Guo and Parker [29]. In both approaches, the external bearing loading has to be known. Relevant results were issued in the latter quoted paper, regarding the bearing radial and axial stiffness, respectively the obtained radial/axial stiffness–load relationship for both radial cylindrical roller and ball bearings being significantly different from those predicted by Gargiulo's well-known equations [30] (perhaps because these old equations do not take into account the elasticity of bearing rings).

2.2. Stochastic optimization

Stochastic programming is a way of tackling the uncertainty by optimizing the objective function on average and also requiring the satisfaction of the constraints (if there are any) on average [31]. This type of programming is focused on making the most out of the fact that the probability distributions of the involved random variables are known or might be estimated. Therefore, the aim is to find the solution that is feasible for almost all possible realizations of the uncertain variables and maximizes the expectation of the wanted function. The expectation, also known as the expected value, of a function $f(x,\omega)$ depending on a vector of decision variables x and a vector of random variables ω with joint density h_ω, is given by [32]:

$$F(x) = E_\omega[f(x,\omega)] = \int_\Omega f(x,y)h_\omega(y)dy \tag{1}$$

for continuous distributions, where Ω is the domain for ω, or

$$F(x) = E_\omega[f(x,\omega)] = \sum_{i=1}^{N} p_i \cdot f(x,\omega_i) \tag{2}$$

for discrete distributions, where p_i is the probability value for the realization ω_i of the vector ω, $i = 1,2,\ldots,N$, and N is the number of possible combinations of the random variable values contained in ω.

In general, stochastic programming models can be solved using different methods and the solution needs to be analyzed and interpreted in order to provide useful information to the decision-maker. A general formulation for the stochastic programming problem is [31]:

$$\min_x E_\omega[f(x,\omega)] \tag{3}$$

subjected to:

$$E_\omega[g_i(x,\omega)] \le 0, \quad i = 1,2,\ldots,m \tag{4}$$

where f is the objective function and g_i are the constraint functions, $i = 1,2,\ldots m$.

2.3. Cuckoo Search algorithm

Cuckoo Search (CS) is a population-based algorithm inspired by the breeding behavior of some cuckoo species. These birds are known for their distinctive and loud *koo-koo* calls, but also for their aggressive mating approach. They all migrate towards better places (with better food and better nests) where they lay their eggs. Some cuckoo species, such as *Ani* and *Guira*, stand out due to the fact that they made the habit of laying their eggs in communal nests. Sometimes they even remove the eggs laid by other cuckoos in order to increase the probability that their own eggs will hatch.

CS algorithm has been developed in 2009 by Xin-She Yang and Suash Deb [33] and it is based on the so-called Lévy flights. It has been observed that, in nature, animals have a random and quasi-random manner of searching for food. In general, the path described while searching for food is a chaotic one with no apparent order [34]. But actually, the direction where the search is headed from the current position can be modeled based on a probability function. Lévy flights are a category of random walks specific to certain insects. Due to the fact that in nature this behavior has been a successful one, it has been embraced in optimum search algorithms. Lévy flights, named after the French mathematician Paul Lévy, provide random walks with a random step length drawn from a Lévy distribution [33], also called stable distribution [34]:

$$Lévy \sim u = t^{-\lambda}, 1 < \lambda \le 3 \tag{5}$$

which has an infinite variance with an infinite mean. These steps actually generate “a random walk process with a power-law step-length distribution with a heavy tail” [33] which can be described as clusters of small steps separated by dramatic jumps.

The random walk using Lévy flights generates a new solution for a certain cuckoo x_i, according to:

$$x_i^{(k+1)} = x_i^{(k)} + \alpha \cdot Lévy(\lambda) \tag{6}$$

where k is the current generation and α is a real positive value representing the step size scaling factor which should be related to the scales of the problem that needs to be solved [35].

3. Application to be optimized

The application depicted in this study consists in a hollow bevel pinion-shaft resting on two similar single-row angular ball bearings (basic designation 7048) in back-to-back (O-) arrangement (Fig. 1a). The shaft is driven by a V-belt drive at a speed of 500 rpm. The driven pulley is mounted on the shaft end by means of a key which is not shown in Fig. 1a. A certain bending force will load the shaft in node 1, due to the necessary belt tension. The reference points of the bearings are 5 and 8, respectively, and the large tapered half bevel pinion is discretized in three frustums of cone which in the analysis were considered as cylinders with the outer diameters equal to the mean diameters of the corresponding respective portions. The shaft geometry can be observed in Fig. 1a and the shaft loading in two perpendicular planes is detailed in Fig. 1b (the horizontal plane) and Fig. 1c (the vertical plane) and the values are provided in Table 1.

The shaft is manufactured of chromium steel and the housing is made of gray cast iron. The information about lubricant and lubrication system is displayed in Table 3. The considered values of the basic static and dynamic radial load ratings of both bearings are $C_r = 260$ kN and $C_{0r} = 375$ kN, respectively. Regarding the bearing seats, it was considered that the outer surfaces of shaft journals are ground and the roughness is $R_{as} = 0.8$ μm. The same roughness (i.e. $R_{aH} = 0.8$ μm) was accepted for the housing bore surfaces. The tolerance of the shaft journal diameter is m6 and the tolerance of the housing bore diameter is H7 (same for both bearings). Furthermore, it should be mentioned that the spacers between the inner and outer rings of the two bearings (Fig. 1a) are ground so that an axial bench preload/clearance is achieved.

An important parameter that influences the bearing arrangement life is the operating temperature. For example, for this application if the bearing operating temperature is considered the ball temperature, namely 90 °C, the bearing temperature follows the distribution given in Fig. 2. It has to be mentioned here that the employed model implies a linear temperature drop or increase between the known temperatures of the limiting surfaces of a certain part. For different operating conditions similar bearing temperature distributions as the one in Fig. 2 are generated. Other parameters that influence the bearing arrangement life besides the temperature are the mounting preloads/clearances of each bearing. Again, as an example, for a working temperature of 90 °C, an interference between the shaft and the bearing inner ring bore of −42.5 μm, and a clearance between the housing bore and the bearing outer ring of 42.5 μm (most probable theoretical values), the coordinates of the groove centers of both inner and outer rings were computed and are given in Table 2 (the upper sign refers to bearing 1 and the lower to bearing 2).

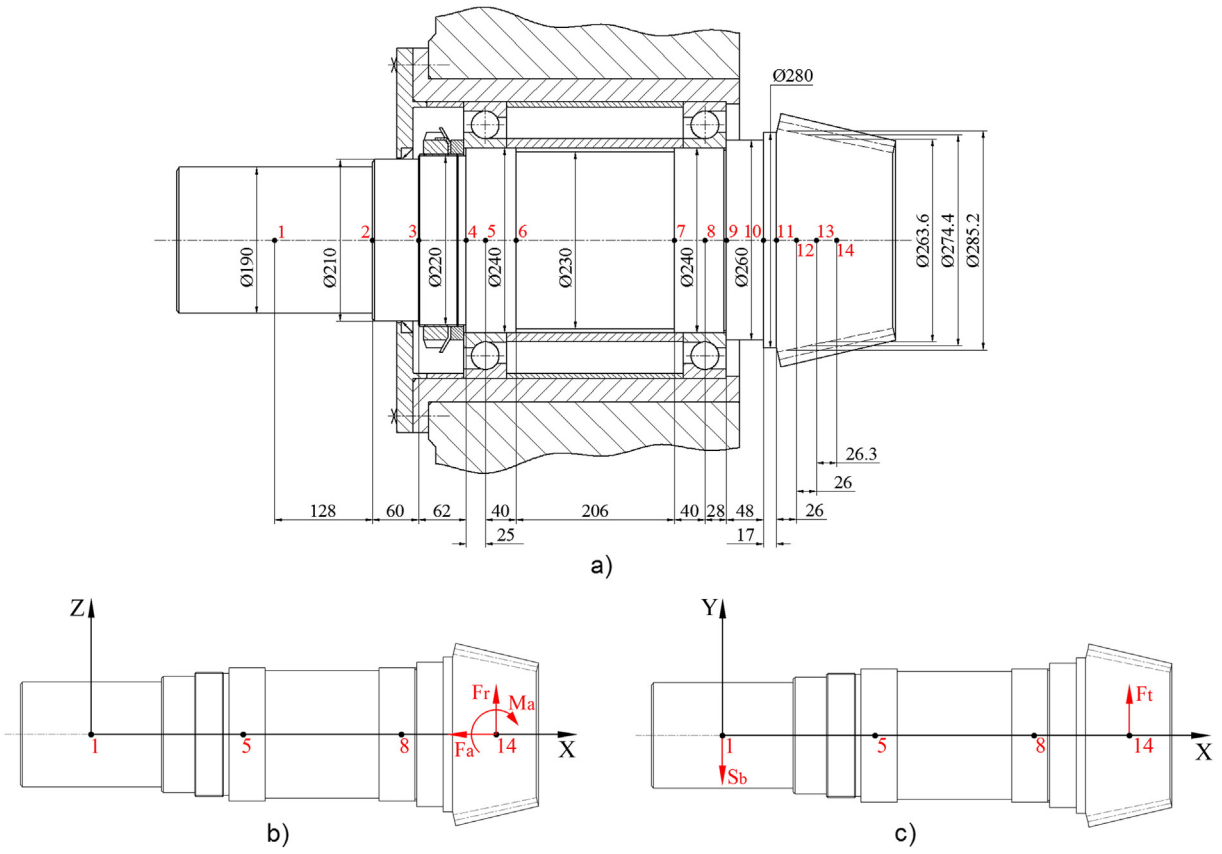

Fig. 1. Shaft supported by two single-row angular ball bearings in back-to-back (O-) arrangement: a) sub-assembly axial section; b) shaft loading in the horizontal plane; c) shaft loading in the vertical plane.

Table 1
Shaft loading.

Plane	Loading	Value
Horiz.	Bevel pinion radial force, kN	13.128
XOZ	Bevel pinion axial force, kN	−2.916
	Moment of the bevel pinion axial force, kN·mm	113.105
Vert.	Belt load, kN	36.929
XOY	Bevel pinion tangential force, kN	−43.654

Obviously, these changes in the coordinates of the ring groove centers determine the change in the preload/clearance of the bench bearing arrangement.

The question that will arise naturally is: what value of the preload/clearance will get the maximum life of the bearings? We ran the program developed based on the bearing load model proposed in this paper for values between −130 μm (preload) and +50 μm (clearance) with a step of 5 μm and the results in terms of bearing modified lives (according to [37]) were plotted in Fig. 3. The values of the interference between shaft and bearing bore, the clearance between the outer ring and housing bore were set at their maximum probable values, and the bearing working temperature was considered 90 °C. It can be easily noticed that in these conditions the maximum bearing arrangement life will be attained if the bearing arrangement is set at −60 μm (preload).

Such an approach may be sufficient for a project that is not very important and/or sophisticated or when the values of the abovementioned interferences/clearances are known but for the production of large amounts of assemblies destined to work in different applications it is no longer valid, because the interferences, clearances and working temperatures are random variables subjected to more or less known laws of distribution.

4. Ball bearing life model

Unlike the procedure recommended by ISO 281:2007 [38], according to ISO 16281:2008 [37] the values of the compressive loads acting on each ball of the bearing are crucial in ball bearing life calculation. Any reference to the bearing life will hereinafter be considered as a reference to the modified rating life of the bearing as provided by ISO 16281:2008. As one can see in the appendices the ball compressive loads are functions of the ball deformations and these are in turn functions of the relative displacements of the inner ring with respect to the outer ring. Consequently, the first goal to be achieved is to find the linear and angular displacements of the bearing reference points.

The concept lying behind the proposed method for calculating these displacements is based on a systemic approach: when the static equilibrium of the shaft is reached, the loads and moments transmitted from the shaft to the bearings (vector $\mathbf{FM}(\Delta\Theta)$) must be reacted by the loads and moments arisen due to the elastic deformations of the rolling elements (vector $\mathbf{fm}(\Delta\Theta)$):

$$\mathbf{FM}(\Delta\Theta) + \mathbf{fm}(\Delta\Theta) = 0 \tag{7}$$

In the proposed approach, the former are obtained using the slope-deflection method (very likely never used before in this context), and the latter result from a certain load-deformation model of rolling elements of the bearing. Thus, the unknowns of

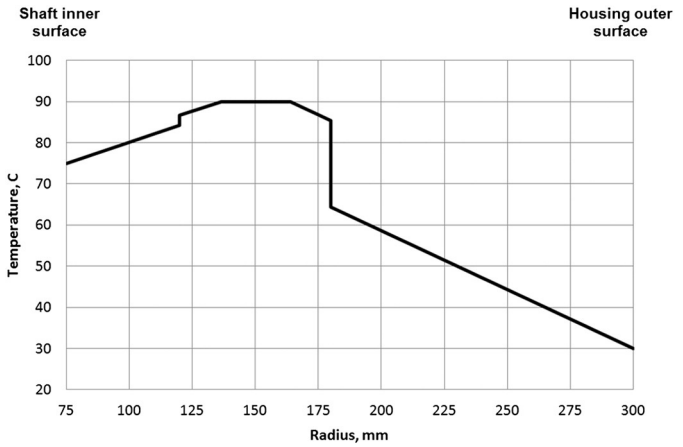

Fig. 2. Bearing temperature distribution.

Table 2
Coordinates (in own systems) of the bearing ring groove centers.

Status	Coordinates of the groove center of the				Contact angle α [rad]]
	Inner ring		Outer ring		
	r_{O_i} [mm]	x_{O_i} [mm]	r_{O_e} [mm]	x_{O_e} [mm]	
Theoretic[1]	150.404	±0.339	149.328	∓0.564	±0.698
After mounting[2]	150.428	±0.369	149.338	∓0.564	±0.708
In operation[3]	150.524	±0.369	149.406	∓0.480[4]	±0.650[5]

[1] At a reference temperature of 20 °C.
[2] Taking into account the mounting temperature of 25 °C.
[3] At the working temperature; the bearing loading is not considered.
[4] The inner ring is considered fixed and the outer ring is displaced with the difference between the thermal expansion of the shaft and housing.
[5] The decrease is caused mainly by the thermal axial expansion of the shaft.

Eq. (7) are the displacements δ and the rotations θ of the shaft support reference points (nodes k_1 and k_2—see Fig. 4) given by

$$\Delta\Theta = \left(\delta_x \delta_{y_{k_1}} \delta_{z_{k_1}} \theta_{y_{k_1}} \theta_{z_{k_1}} \delta_{y_{k_2}} \delta_{z_{k_2}} \theta_{y_{k_2}} \theta_{z_{k_2}}\right)^T \tag{8}$$

which are determined first by solving the equations of equilibrium. Once these displacements are found, the unknown forces are obtained through force–displacement relations. Please note that nodes k_1 and k_2 correspond to nodes 5 and 8, respectively, from the particular case of the shaft rested on two bearings presented in Section 3. The procedure by which Eq. (7) is aggregated is presented in detail in Appendix A and Appendix B.

By solving through an iterative method the set of simultaneous Eq. (7), the vector $\Delta\Theta$ is obtained and it can be easily disaggregated in two displacement vectors corresponding to each bearing ($\delta\theta$ vectors in Appendix A). With these the deformation of each ball of each bearing is calculated and therefore, the corresponding compressive loads are obtained (see Appendix B). From this point the bearing life calculation follows with no difficulties the procedure from ISO 16281:2008.

It has to be mentioned here that number of unknowns of the system of nonlinear equations that results from the static equilibrium condition depends on the number of bearings and not on the number of discretization nodes. Moreover, the matrices involved in the solving process depend only on the shaft (geometry and material) and its loading. All these transform the computation into a facile one, no matter how complicated the shape of the shaft and its loading is.

For the particular case of the application presented in Section 3 in which the shaft was defined using 14 nodes, a system of 70 non-linear simultaneous equations with 70 unknowns is obtained if one uses FEA. However, using the method proposed in this paper there are only 9 simultaneous equations with 9 unknowns. Considering that the solving of the system of simultaneous equations has to be performed at every step of the optimization algorithm when the objective function is called, the model proposed in this paper becomes more advantageous with respect to a FEA-based model.

5. Optimization tool

In order to efficiently solve the proposed optimal design problem under uncertainty we chose CS algorithm. The standard version of CS that uses cuckoo migration based on Lévy flights was modified so that it manages to make a tradeoff between exploitation and exploration. The algorithm was improved based on the idea that with greater knowledge, less exploration is necessary. For this reason, the evolution of the knowledge accumulated by the cuckoo population during migration was measured in an original manner based on the Knowledge Gradient policy (KG). We call this enhanced algorithm KGCS. The pseudocode of the improved CS algorithm is given in Fig. 5.

The algorithm was redesigned with two well delimited phases. The first phase is focused on exploring the search space while in the second phase the degree of exploration is reduced and the degree of exploitation is increased.

Table 3
Lubricating conditions.

Parameter	Value
Kinematic viscosity of oil at 40 °C, mm^2/s	80
Kinematic viscosity of oil at 100 °C, mm^2/s	8.6
EP additives	No
Lubrication type	Oil lubrication without filtration
Cleanliness codes ([36])	−/15/12
Reference kinematic viscosity of oil, mm^2/s	14.95
Kinematic viscosity of oil at working temperature, mm^2/s	11.20
Viscosity ratio	0.75

Table 4
Standard CS vs. KGCS — test results.

Function	Average required number of objective function evaluations applying standard CS	Average required number of objective function evaluations applying KGCS	Difference	% difference
Rosenbrock	205,178.6	190,621.4	14,557.2	7.09%
Griewank	199,214.3	186,350.5	12,863.8	6.46%
Ackley	177,571.4	168,978.6	8592.8	4.84%

In order to achieve an increased level of exploration in the first phase, KGCS uses three cuckoo populations. They are initially randomly generated within the bounds of the search space and evaluated by calculating the fitness for each cuckoo. The three populations explore the search space and try identifying the best solution independently. The exploration process is based on laying eggs using Lévy flights and lasts for several generations. During the exploration phase an archive with the best cuckoos is updated for each population at the end of each generation. Tests have shown that the level of 5%–10% from the maximum allowed number of generations is a good end condition for the first phase.

When the exploration phase has ended, the value of the gradient is computed according to the KG policy for each population based on its own archive containing the best cuckoos obtained so far. The detailed mathematical model on which the implementation of gradient was based is presented in [39].

In the second phase, the migration process towards the optimal solution is conducted only by the population which proved to be the best and which ensures the largest expected improvement when estimating the best reward according to KG policy. The end condition of the second phase consists in reaching the maximum allowed number of generations.

The KGCS algorithm was tested on some benchmark functions such as Rosenbrock, Griewank, and Ackley's function. The evolution of the populations was monitored during the two phases of the algorithm for each of the tested functions. An intense exploration of the search space was observed during the first phase, while the second phase was characterized by an increased level of convergence. The improved algorithm was tested 10 times on each of the mentioned benchmark functions. The results are summarized in Table 4.

When comparing the results obtained using KGCS algorithm to the ones obtained using the standard version of CS algorithm, it has to be mentioned that both algorithms have a percentage of identifying the global optimum of 100%. However, there is a decrease of the number of evaluations required to find the global optimum when using KGCS that is presented in Table 4.

The average decrease of the number of required objective function evaluations caused by using KGCS is about 12,005 evaluations, which means a percentage decrease of 6.13% from the number of required objective function evaluations when using standard CS. Even if the improvement of 6.13% does not seem to be so important, it can become crucial when it comes to complex optimization functions which require a long running time. Moreover, it is very likely that more runs are required to obtain an accurate solution when the process is governed by randomness and in this case any decrease of the running time is a desirable benefit. Also, the percentage decrease might differ when KGCS is used for other functions. For example, for the optimal design problem approached in this study, the percentage decrease was 13% for the first stage and approximately 17%, for the second and the third stages.

6. Problem formulation

The optimal design of the bearing arrangement presented in Section 3 was addressed from the maximum bearing life standpoint. The aim was to find the optimal bench bearing arrangement preload/clearance that maximizes the bearing arrangement life (minimum bearing life of the two bearings from the considered arrangement — see Fig. 3) calculated according to [37] using the method presented in Section 4.

In order to validate the proposed optimization procedure a simplified problem was first formulated and the bearing arrangement life, denoted hereinafter by L, was expressed as a function of only four variables. The first variable, x, represents the unknown bench bearing arrangement preload/clearance. It was considered to be varying between −110 μm and 5 μm (a negative value refers to bearing arrangement preload, while a positive one refers to bearing arrangement clearance). The other three variables are random variables and they were considered to have the same values for both bearings. The second variable, In, represents the interference between the shaft and the bearing inner ring bore, the third one, Cl, represents the clearance between the housing bore and the bearing outer ring, and the last variable, T, represents the bearing operating temperature. For the considered bearing arrangement, the Gaussian probability distribution for In and Cl was established according to [40] and the

Table 5
Random variable domain and probability distribution.

No.	Variable	Unit	Symbol	Probability distribution
1	Interference	μm	In	$In \sim N(-42.5, 6.07)$
2	Clearance	μm	Cl	$Cl \sim N(42.5, 10.58)$
3	Temperature	°C	T	$T \sim N(70, 6)$

Table 6
Optimization results.

Problem	Stage	Solution [μm]	Standard deviation [μm]
Simplified	I	−55	0.480
	II	−63	0.672
	III	−37	0.443
Real	I	−55	0.792
	II	−65	0.758
	III	−36	0.188

results are given in Table 5 where $N(\mu,\sigma)$ represents the normal distribution with the mean μ and the standard deviation σ. For the random variable that represents the temperature the range is [50; 90] °C and the probability distribution is shown in Table 6. These values were chosen because we consider that it is a suitable proposal that maps on the reality of the working conditions of the application.

Taking into consideration that we deal with a process governed by three random variables, providing an optimal solution as a single value for the unknown x is hard to believe and accept and even harder to put into practice. Hence, an interval-solution is more desirable. In order to obtain both the optimal value for x and the optimal interval-solution, the proposed optimal design problem was formulated as a three-stage optimization problem.

The goal of the first stage is to find the optimal value of the bench bearing arrangement preload/clearance as a single point $x_0, x_0 \in [-110;5]$ μm while maximizing the expected bearing arrangement life. The first-stage problem was formulated as a stochastic maximization problem:

$$\max_{x\in[-110;5]} \frac{1}{nrT}\cdot\sum_{i=1}^{nrT} L(x, In(i), Cl(i), T(i)) \tag{9}$$

where nrT represents the sample size in the Monte Carlo Sampling (MCS) used to approximate the expected value of the bearing arrangement life. The sample consists of triplets containing values for interference, $In(i)$, clearance, $Cl(i)$, and temperature, $T(i)$. These values are randomly generated according to their own probability distribution (Table 5). Since there is no risk of confusion, the simplifying notation using only the variable i will be hereinafter used to refer to the triplet $(In(i), Cl(i), T(i))$.

The last two stages of the optimization aim to find the optimal solution as the largest interval of convenient solutions. For a given triplet the maximum bearing arrangement life is obtained for a value x_m of the bench bearing arrangement preload/clearance. We define a convenient solution x_c as the value for which the bearing arrangement life is at least 95% from the maximum life obtained for x_m. For the example given in Fig. 3, x_m is −60 μm and the convenient solutions are from −80 μm to −30 μm. Consequently, a value x_c, $x_c \in [-110;5]$, is a convenient solution if $L(x_c, In, Cl, T) \geq 0.95 \cdot L(x_m, In, Cl, T)$, where x_m is the value that maximizes $L(x, In, Cl, T)$ for a given triplet $(In, Cl, T) \in [-68;-17]\times[0;85]\times[50;90]$. Obviously, the convenient solutions for a given triplet lay into a range containing x_m.

Introducing $p, q \in [0;1]$, we define the following two functions that will be used in the search for the lower and upper margins of the convenient solution set:

$$low : [0;1] \to [-110; x_0], \quad low(p) = x_0(1-p) - 110p \tag{10}$$

$$up : [0;1] \to [x_0; 5], \quad up(q) = x_0(1-q) + 5q \tag{11}$$

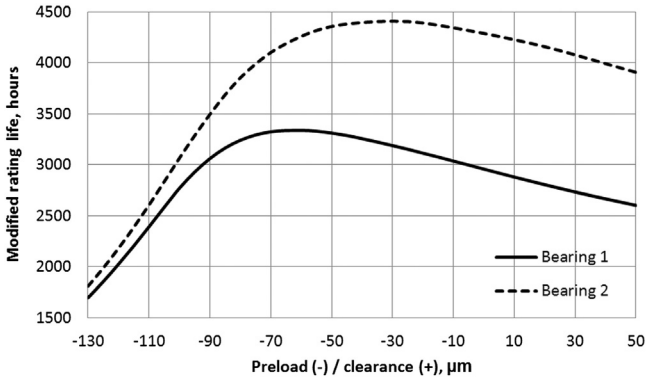

Fig. 3. Modified bearing lives vs. bench bearing arrangement preload/clearance.

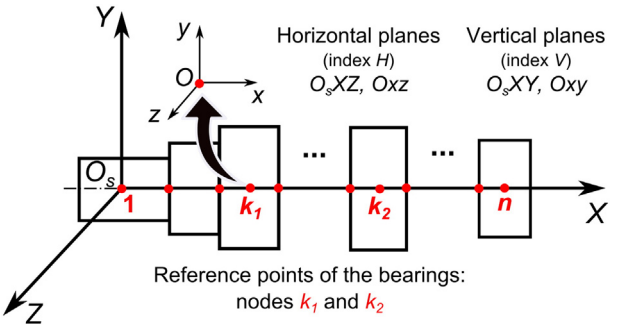

Fig. 4. Cartesian global and local systems of coordinates referring to the shaft and bearings.

KGCS algorithm:

```
begin
    generate three initial populations of cuckoos
    evaluate the fitness of each cuckoo from each population
    save the best cuckoo so far for each generation in its own archive
    initialize generational counter k to 0
    while (k < 5% · Nmax)
        for each population
            for each cuckoo in the population
                generate a new cuckoo using Lévy flights
                evaluate the fitness of the new cuckoo
                if the obtained fitness is larger than the parent fitness
                    replace the parent with the new cuckoo
                end if
            end for
            replace a fraction pa of the cuckoos with new ones
            evaluate the new cuckoos
            update the archive with the best cuckoos
            update generational counter k
        end for
    end while
    compute knowledge gradient for each population based on its own archive
    choose population with the largest knowledge gradient
    find the best cuckoo obtained so far for the chosen population
    while (k < Nmax)
        for each cuckoo in the chosen population
            generate a new cuckoo using Lévy flights
            evaluate the fitness of the new cuckoo
            if the obtained fitness is larger than the parent fitness
                replace parent with the new cuckoo
            end if
        end for
        replace a fraction pa of the cuckoos with new ones
        evaluate the new cuckoos
        update the best cuckoo obtained so far
      update generational counter k
    end while
return the best cuckoo
end
```

Fig. 5. KGCS pseudocode.

In order to find the lower margin which represents the minimum allowed convenient bench bearing arrangement preload/clearance, the following problem was formulated:

$$\min_{p\in[0;1]} \lambda\sum_{i=1}^{nrT}[0.95\cdot L(x_0,i)-L_{low}(p,i)]+\frac{1}{p} \tag{12}$$

where λ is a penalty coefficient whose purpose is to penalize all values that are not convenient solutions for all generated triplets. By using a penalty coefficient, the search is directed first towards the range containing convenient solutions. In order to ensure that the obtained value is indeed the minimum allowed convenient solution for all randomly generated triplets the ratio $1/p$ was introduced in Eq. (12). The aim is to maximize p because a larger value of p corresponds to a lower value for the lower margin of the solution set. The function L_{low} is used to express the utility brought by a value *low* (p) and its functional form is based on the idea that all convenient solutions are contained in the interval-solution and therefore, in this stage they offer us the same utility as the value x_0 that maximizes the bearing arrangement life. This function is given by:

$$L_{low}(p,i)=\begin{cases} 0.95L(x_0,i), & if\ \ L(low(p),i)\geq 0.95L(x_0,i) \\ L(low(p),i), & otherwise \end{cases} \tag{13}$$

The third stage of the conducted optimization consists in finding the upper margin of the solution set which represents the maximum allowed convenient bench bearing arrangement preload/clearance. In order to achieve this, the optimization problem for the third stage was formulated as follows:

$$\min_{q\in[0;1]} \lambda\sum_{i=1}^{nrT}\left[0.95\cdot L(x_0,i)-L_{up}(q,i)\right]+\frac{1}{q} \tag{14}$$

where λ is a penalty factor with the same purpose as before. The ratio $1/q$ was introduced in Eq. (14) to ensure the largest value for the upper margin of the solution set. The aim is to maximize q because a larger value of q corresponds to a larger value for the upper margin of the solution set of convenient solutions. The function L_{up}, similar to L_{low}, is used to express the utility brought by a value $up(q)$:

$$L_{up}(q,i)=\begin{cases} 0.95L(x_0,i), & if\ \ L(up(q),i)\geq 0.95L(x_0,i) \\ L(up(q),i), & otherwise \end{cases} \tag{15}$$

7. Optimization results

For all three stages of the conducted optimization using KGCS, 500 triplets per cuckoo generation were used and 225,000 evaluations of the objective function were allowed. Particularly, for the second and the third stages of the optimization, the penalty factor λ was set to 10^{10} and x_0 was set to −55 μm, the optimal value of the bench bearing arrangement preload obtained in the first stage.

The optimal values resulted at each stage are provided in Table 6 as the average solutions obtained from 10 trials per stage. To have a fair time comparison we adopted the average running time required for the entire optimization as the unit of time, UT (about 18 min for an Intel Core™ i7-3632QM, 6 MB Cache, 2.20 GHz processor and an installed memory of 8 GB RAM). The average running times required for stages I, II, and III are 0.17 UT, 0.42 UT, and 0.41 UT, respectively.

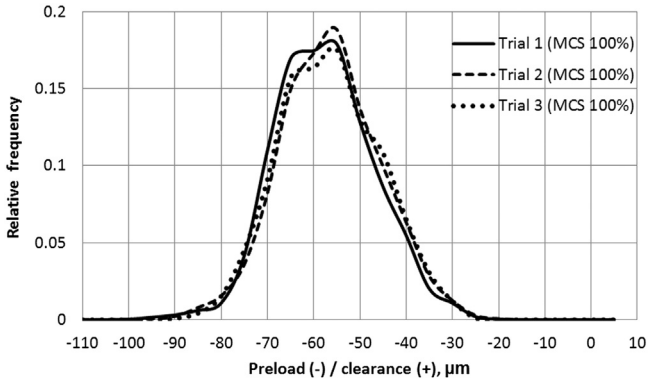

Fig. 6. Distributions obtained using MCS 100%.

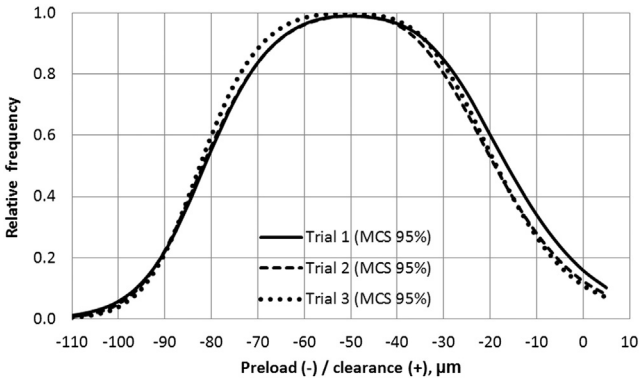

Fig. 7. Distributions obtained using MCS 95%.

In order to validate the results obtained using KGCS, MCS was chosen as an estimation tool and it was used for two different types of estimations. The first estimation, corresponding to the first stage of the conducted optimization, was called MCS 100%. For each of the three random variables (*In*, *Cl*, and *T*), 125 values were generated according to their distributions (Table 5) and then, all possible combinations were considered. For each combination the solution was found as the bench bearing arrangement preload/clearance x that maximizes the bearing life function, where $x \in \{-110, -105, ..., 0, 5\}$ μm. MCS 100% was repeated 3 times and each time the relative frequency (the number of appearances as solution divided by the sample size) of the obtained solutions was computed. The three MCS 100% distributions can be observed in Fig. 6.

The average of the means of the three distributions is −56.8732 μm and the average computing time was 49 UT (almost 15 h on the same machine). When comparing the estimation results to the optimization ones, if one takes into consideration that all the variables were randomly generated, it can be stated that the difference between the solution from the first stage of the optimization and the obtained average mean of the three MCS 100% is insignificant. However, the time difference, well reflected by the time ratio 0.17:49, is huge.

The second estimation, corresponding to the second and the third stages of the conducted optimization, was called MCS 95% and its purpose was to estimate the solution of the optimization problem as an interval. The sample for this type of estimation was obtained similarly to the MCS 100% sample, but this time using only 100 values per variable. The convenient solutions (as defined in Section 6) were found for each sample triplet and their relative frequencies were calculated (see Fig. 7). MCS 95% was repeated three times requiring an average computing time of 30 UT.

As it can be observed in Fig. 7, in this type of estimation the distribution peak flattened, providing the solution not as a single point, but as an interval of convenient solutions. The values with a relative frequency higher than 0.95 have been considered to be part of the interval-solution. Therefore, the estimated interval containing convenient solutions obtained using MCS 95% is [−60; −40] μm. This interval is insignificantly narrower than the interval [−63; −37] μm, obtained from the proposed three-stage optimization performed using KGCS. Though, the time ratio 0.83:30 indicates a considerable time difference. It should be mentioned here that a finer discretization (with a step lower than 5 μm) of the interval representing the values of the bench bearing arrangement preload/clearance could lead to a larger interval-solution when using MCS 95%, but it would also dramatically increase the average computing time. It has to be mentioned here that the estimated time needed to validate the solution of the real problem is about 100 times larger for the same accuracy. This determined us to present the formulation of the simplified problem and validate the obtained solution.

An attempt was made to replace the last two stages with only one stage in which the search for both interval-solution limits was conducted at once. The obtained results were similar but with a much larger standard deviation for the same number of objective function evaluations. Therefore, the three-stage approach was considered appropriate and the abovementioned simplification of the problem was removed. In this way the real problem is described by six variables: x, *In*1, *In*2, *Cl*1, *Cl*2, and *T*, where 1 and 2 refer to the first and second bearings, respectively. The optimization results are given in Table 6 and consequently, it can be stated that the bench bearing preload should be in the interval [−65; −36] μm.

8. Conclusions

This study is focused on finding the optimal value of the bench bearing preload/clearance that maximizes the bearing arrangement life which depends on geometric and operating parameters treated here as random variables with known distributions. A new systemic approach for bearing ball load calculation was used for bearing arrangement life computation.

The optimal design problem was formulated as a three-stage optimization problem. The first stage consisted in the stochastic optimization problem of finding the value of the bench bearing arrangement preload/clearance that maximizes the expected bearing arrangement life. The second and the third stages aimed to find the solution to the proposed problem as an interval.

The new KGCS algorithm was used to find the optimal bearing arrangement which was validated using MCS. In contrast to MCS, which proved to be a highly time-consuming estimation tool, KGCS proved to be flexible, accurate, and with a low computational cost.

The difference between the obtained solutions for the simplified and the real problem, respectively, is relatively small. This suggests that the simplified approach can be used in common applications which do not require a high degree of accuracy.

Acknowledgments

The authors would like to thank the RKB Group, the Swiss bearing manufacturer, for the permission to publish these results and the RKB staff for their great interest and support during the development of this project.

Appendix A. Loads and moments transmitted from the shaft to the bearings

A shaft is initially considered in Fig. A.8 and n, as the number of discretization nodes. The nodes could represent supports, points where external loads and moments are applied, points at which the shaft changes its section, etc. Each shaft element (segment) i, $i+1$ is characterized by its length L_i and moment of inertia I_i.

An external load F_i and an external bending moment M_i could act in each node i of the shaft. Please note that the present paper does not concern distributed loads and moments but, for example, if a distributed load exists, it can be equivalated with a concentrated load applied at the center of the mass of the distributed load. The positive directions of the loads and moments are those indicated in Fig. A.9:

$$FM = (F_1 \;\; F_2 \;\; \ldots \;\; F_n M_1 M_2 \ldots M_n)^T \tag{A.1}$$

The slope-deflection equations establish force–displacement relationships for the beam element [41]:

$$\mathcal{F}_{i,i+1} = 6\left(2c_i\delta_i - 2c_i\delta_{i+1} + b_i\theta_i + b_i\theta_{i+1}\right) + \mathcal{F}^F_{i,i+1} \tag{A.2}$$

$$\mathcal{F}_{i+1,i} = -6\left(2c_i\delta_i - 2c_i\delta_{i+1} + b_i\theta_i + b_i\theta_{i+1}\right) + \mathcal{F}^F_{i+1,i} \tag{A.3}$$

$$\mathcal{M}_{i,i+1} = -2\left(3b_i\delta_i - 3b_i\delta_{i+1} + 2a_i\theta_i + a_i\theta_{i+1}\right) + \mathcal{M}^F_{i,i+1} \tag{A.4}$$

$$\mathcal{M}_{i+1,i} = -2\left(3b_i\delta_i - 3b_i\delta_{i+1} + a_i\theta_i + 2a_i\theta_{i+1}\right) + \mathcal{M}^F_{i+1,i} \tag{A.5}$$

in which $\mathcal{M}^F_{i,i+1}$ and $\mathcal{M}^F_{i+1,i}$ are fixed-end moments, $\mathcal{F}^F_{i,i+1}$ and $\mathcal{F}^F_{i+1,i}$ are fixed-end shear forces, and

$$a_i = E_s \cdot \frac{I_i}{L_i};\; b_i = \frac{a_i}{L_i};\; c_i = \frac{b_i}{L_i},\; i = 1, \ldots, n-1 \tag{A.6}$$

With respect to the fixed-end shear forces and moments (Fig. A.10), the following new vector can be defined:

$$RrM = (R_1 \;\ldots\; R_n rM_1 \ldots rM_n)^T \tag{A.7}$$

and its elements, obtained by summing the corresponding Eqs. (A.2)–(A.5) in each node.

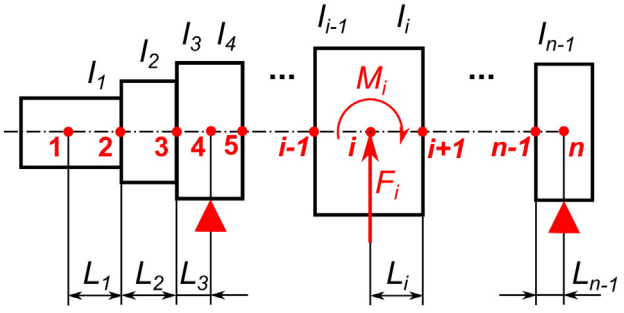

Fig. A.8. Shaft discretization.

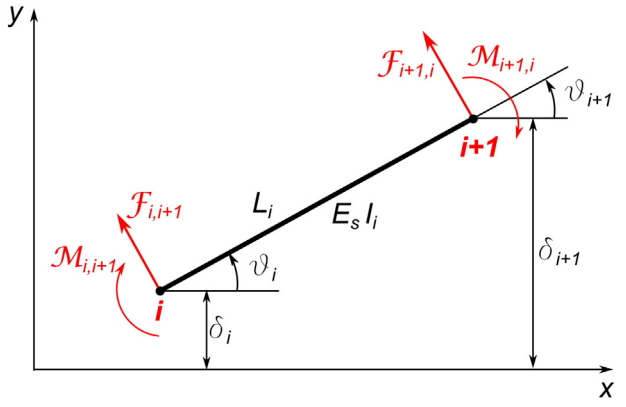

Fig. A.9. Slope and deflection of a shaft element.

Using the following denotation $\delta\theta = (\delta_1 \quad \ldots \quad \delta_n \theta_1 \quad \ldots \quad \theta_n)^T$, one obtains the succeeding matrix equation:

$$RrM = AG \cdot \delta\theta - FM \tag{A.8}$$

where AG is the stiffness matrix. It is worth noting that if i is a free node, then $RrM_i = R_i = 0$ and $RrM_{n+i} = rM_i = 0$. If i is a support, then RrM_i and RrM_{n+i} could be non-zero, according to the support type and represents the reaction and the reaction moment of the support against the shaft.

Presuming that the following q nodes $q_1, q_2 \ \ldots, \ q_q$ are the shaft supports (in ascending order) let's extract the vector $\delta\theta^{(p)} = (\delta_{q_1} \ \ldots \ \delta_{q_q} \ \ \theta_{n+q_1} \ \ldots \ \theta_{n+q_q})^T$ from the vector $\delta\theta$ and let's symbolize the remaining vector with $\delta\theta^{(s)}$. We introduce two new matrices $AG^{(s)}$ and $AG^{(p)}$: $AG^{(s)}$ results from the matrix AG by erasing the columns $q_1, q_2 \ \ldots, \ q_q, \ n+q_1, \ n+q_2 \ \ldots \ n+q_q$ and $AG^{(p)}$ will be formed by the erased columns. Eq. (A.8) becomes:

$$RrM = AG^{(p)} \cdot \delta\theta^{(p)} + AG^{(s)} \cdot \delta\theta^{(s)} - FM \tag{A.9}$$

The system is separated into two systems corresponding to the constrained and free nodes, and the equations for RrM_{free} and $RrM_{constrained}$ can be written using Eq. (A.9), for example:

$$RrM_{free} = AG^{(p)}_{free} \cdot \delta\theta^{(p)} + AG^{(s)}_{free} \cdot \delta\theta^{(s)} - FM_{free} \tag{A.10}$$

RrM_{free} corresponds to the free nodes, and therefore this vector is null. The matrices $AG^{(p)}_{free}$ and $AG^{(s)}_{free}$ are deduced from the matrices $AG^{(p)}$ and $AG^{(s)}$, respectively, by erasing the rows $q_1, \ \ldots, \ q_q, n+q_1 \ \ldots, n+q_q$. The matrices $AG^{(p)}_{constrained}$ and $AG^{(s)}_{constrained}$ are formed by the erased rows. FM_{free} is obtained from FM by erasing the rows $q_1 \ \ldots, \ q_q, \ n+q_1 \ \ldots, \ n+q_q$, while $FM_{constrained}$ is formed by the erased rows. Expressing the elements of the vector $\delta\theta^{(s)}$ as a linear combination of the

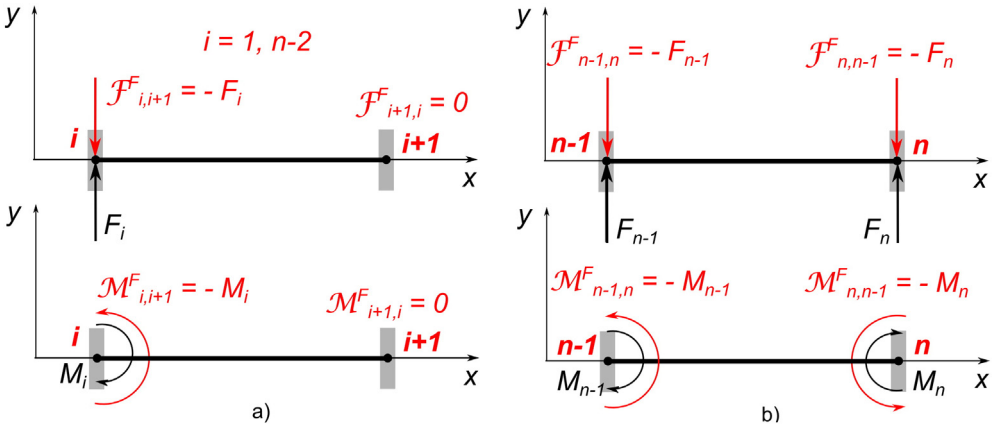

Fig. A.10. Fixed-end shear forces and moments: a) first $n-2$ segments; b) last segment.

elements of the vector $\delta\theta^{(p)}$ from Eq. (A.10) and substituting them in the equation corresponding to the constrained nodes, it yields:

$$RrM_{constrained} = A \cdot \delta\theta^{(p)} + B \tag{A.11}$$

where

$$A = AG^{(p)}_{constrained} - AG^{*(s)} \cdot AG^{(p)}_{free}$$
$$B = AG^{*(s)} \cdot FM_{free} - FM_{constrained}$$
$$AG^{*(s)} = AG^{(s)}_{constrained} \cdot \left(AG^{(s)}_{free}\right)^{-1}$$

Using Eq. (A.11) the corresponding equations can be written for the vertical and horizontal plane in which the loads and the moments transmitted from the shaft to the bearings occur. Aggregating these equations and considering both bearings on which the shaft is rested on as well as the axial force, the vector *FM* can be found by changing the sign of the reactions and reaction moments:

$$\mathbf{FM} = \mathbf{A} \cdot \Delta\Theta + \mathbf{B} + \mathbf{FA} \tag{A.12}$$

where $\mathbf{FA} = (F_a\ 0\ 0\ 0\ 0\ 0\ 0\ 0\ )^T$ and F_a is the axial force.

Appendix B. Loads and moments transmitted to the shaft due to the bearing elastic deformations

The model created is relatively similar to that presented in [15], yet with notable differences. For the rolling bearing analysis, one can consider the relative movement between the bearing rings.

In order to limit the model complexity and following the most frequently used shafts, housings, and bearing arrangements, the ensuing assumptions are considered: (1) deformations of the shaft, housing and bearing rings are neglected and only the elastic deformations of the rolling elements are included; (2) centrifugal forces acting on the rolling elements, loads generated by interaction from the cage, frictional forces inside the bearings, and gyroscopic moments are neglected; (3) spring constants of the balls are equal and constant with temperature.

Two coordinate systems were introduced, to facilitate the analysis in the bearing reference point: a right-handed Cartesian one (*Oxyz*, in Fig. B.11) and a cylindrical system *Oφx*, where φ is the angle between the *r*-axis and positive *y*-direction, being positive if measured as depicted in Fig. B.11.

Let the inner ring displacement vector be symbolized by $\delta\theta = (\delta_x\ \delta_y\ \delta_z\ \theta_y\ \theta_z\ )^T$ and the loading from the rolling elements on the inner ring by $fm = (f_x\ f_y\ f_z\ m_x\ m_y\ )^T$. All loads and displacements refer to the bearing reference point O. Now consider an inner ring axial section, positioned to such angle φ chosen so that the *rx*-plane passes through the center of the ball being selected. As it will be noticed, the analysis can be simplified by choosing the inner ring groove center O_i (Fig. B.11) as reference point of the selected inner ring axial section. This point will be stored as the following vector: $O_i = (r_{O_i}\ x_{O_i})^T$. The abovementioned axial section is loaded (by the ball deformation) in its reference point O_i by the load vector $\mathcal{QT}$, where $\mathcal{QT} = (\mathcal{Q}_r\ \mathcal{Q}_x\ \mathcal{T}_\varphi)^T$, corresponding to the displacement vector $u\gamma$, where $u\gamma = (u_r\ u_x\ \gamma_\varphi)^T$. Since O_i was chosen as reference point of the axial section, it results that always $\mathcal{T}_\varphi = 0$ and vectors $\mathcal{Q}$ and u were used instead of $\mathcal{QT}$ and $u\gamma$, where $\mathcal{Q} = (\mathcal{Q}_r\ \mathcal{Q}_x\ )^T$ and $u = (u_r\ u_x\ )^T$.

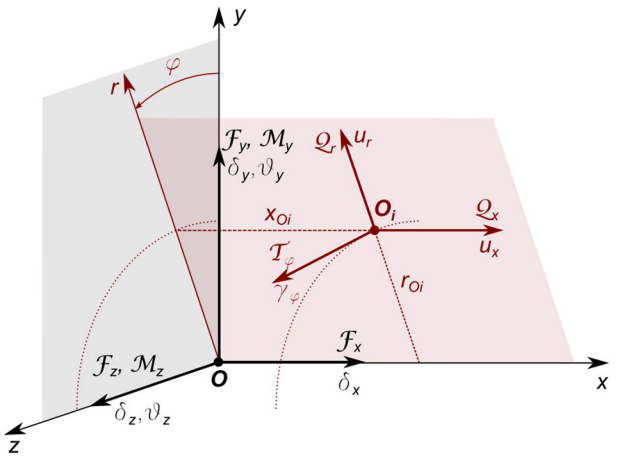

Fig. B.11. Bearing Cartesian and cylindrical coordinate systems. Inner ring loading and displacements.

The situation becomes more complicated for roller bearings [20,21,42] and, at least other criteria determine the choice of the reference point of the inner ring axial section [16].

As the displacements are usually small, the displacement vectors u and $\delta\theta$ can be related using $u = T_{xyz2rx}(O_i,\varphi)\cdot\delta\theta$, where the transformation matrix T_{xyz2rx} (O_i,φ) is given by the equation:

$$T_{xyz2rx}(O_i,\varphi) = \begin{pmatrix} 0 & \cos\varphi & \sin\varphi & -x_{Oi}\sin\varphi & x_{Oi}\cos\varphi \\ 1 & 0 & 0 & r_{Oi}\sin\varphi & -r_{Oi}\cos\varphi \end{pmatrix} \tag{B.1}$$

and the rolling element force vector $\mathcal{Q}$ is transformed to an equivalent force vector fm at the inner ring reference point using $fm = T_{rx2xyz}(O_i,\varphi)\cdot\mathcal{Q}$, where $T_{rx2xyz}(O_i,\varphi) = [T_{xyz2rx}(O_i,\varphi)]^T$. The load vector $\mathcal{Q}$ and the compressive load Q acting on the ball are related by $\mathcal{Q} = Q\cdot T_{\alpha 2rx}(\alpha)$, where $T_{\alpha 2rx}(\alpha) = (-\cos\alpha - \sin\alpha)^T$ and a is the contact angle (Fig. B.12). Based on classical Hertzian theory $Q = c_P\cdot\delta^{3/2}$, where the c_P is the spring constant. Therefore,

$$\boldsymbol{fm} = c_P\cdot\delta^{3/2}\cdot T_{\alpha 2xyz}(O_i,\varphi,\alpha) \tag{B.2}$$

where $T_{\alpha 2xyz}(O_i,\varphi,\alpha) = T_{rx2xyz}(O_i,\varphi)\cdot T_{\alpha 2rx}(\alpha)$. The previously mentioned axial section through the bearing is presented in more detail in Fig. B.12. In this figure r_i and r_e are the radii of the inner ring and outer ring raceway profiles in the axial plane, respectively, D_w is the ball diameter, and O_e is the outer ring groove center. As O_i, the point O_e is stored by means of the subsequent vector $O_e = (r_{O_e} x_{O_e})^T$.

The total elastic deformation of the ball is obviously $\delta = \max(0, -s' - s'')$. It is very easy to prove that the contact angle and the deformation of the ball are two functions of the position of the bearing rings and therefore, the status of the bearing is uniquely described by the vectors O_i and O_e, respectively.

This approach is extremely helpful also because one can discern between the status of the bearing "before the external loading" (e.g. preload/clearance after mounting) and its status "after the external loading". If the initial status of the bearing is described by the vectors O_i^i and O_e^i the final status (after the external loading of bearing) is depicted by the vectors $O_i^f = O_i^i + u$ and $O_e^f = O_e^i$. Consequently, the values after loading of the contact angle and the ball total elastic deformation can be determined and then used in Eq. (B.3). Therefore, knowing the initial status of the bearing before loading and using the equations presented above for every ball j of those Z balls of the bearing, the loading from the rolling elements on the inner ring will be:

$$fm = c_P\cdot\sum_{j=1}^{Z}\delta_j^{3/2}\cdot T_{\alpha 2xyz}\left(O_i^i + u_j,\varphi_j,\alpha_j\right) \tag{B.3}$$

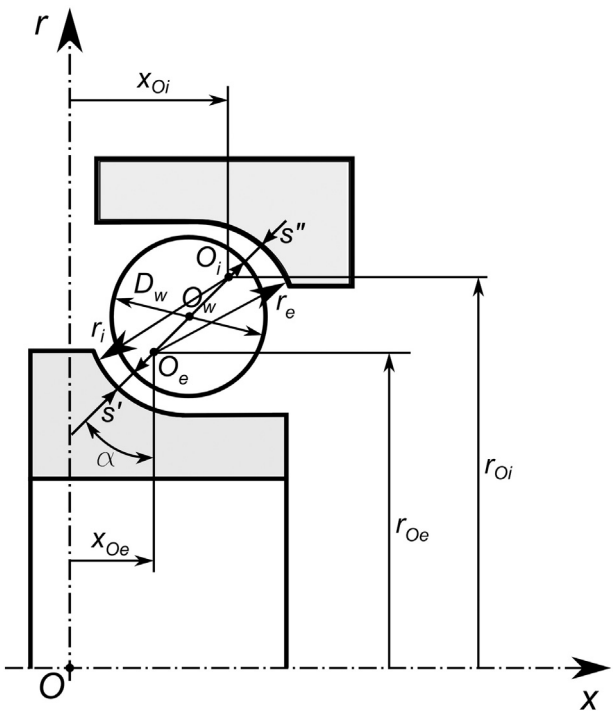

Fig. B.12. Bearing axial section geometry.

It is obvious that for a given initial status of the bearing the vector *fm* is a function of only the displacement vector δθ. Note that in our approach the initial status of the bearing before loading always encompasees the elastic deformation of the bearing rings due to fits and the thermic expansions of the bearing rings and shaft (both radial and axial).

As there are two bearings supporting the shaft in the application presented in Section 3, two equations similar to Eq. (B.3) can be derived. After a convenient aggregation the vector *fm* is obtained as a function of ΔΘ (which contains five displacements per bearing node with the observation that since the axial displacements of each of the two nodes are considered equal in this approach, the corresponding value is considered only once).

References

[1] O. Kocadağl, R. Keskin, A novel portfolio selection model based on fuzzy goal programming with different importance and priorities, Expert Syst. Appl. 42 (20) (2015) 6898–6912.
[2] R.M. Kovacevic, G.C. Pflug, Electricity swing option pricing by stochastic bilevel optimization: a survey and new approaches, Eur. J. Oper. Res. 237 (2) (2014) 389–403.
[3] B. Xu, Z. Lin, Z. Wu, X. Shi, Y. Qiao, G. Luo, Target-oriented overall process optimization (TOPO) for reducing variability in the quality of herbal medicine products, Chemom. Intell. Lab. Syst. 128 (2013) 144–152.
[4] A. Alonso-Ayuso, F. Carvallo, L.F. Escudero, M. Guignard, J. Pi, R. Puranmalka, A. Weintraub, Medium range optimization of copper extraction planning under uncertainty in future copper prices, Eur. J. Oper. Res. 233 (3) (2014) 711–726.
[5] J. Steimel, S. Engell, Conceptual design and optimization of chemical processes under uncertainty by two-stage programming, Comput. Chem. Eng. 81 (2015) 200–217 special Issue: Selected papers from the 8th International Symposium on the Foundations of Computer-Aided Process Design (FOCAPD 2014), July 13-17, 2014, Cle Elum, Washington, {USA}.
[6] K.S. Moghaddam, Fuzzy multi-objective model for supplier selection and order allocation in reverse logistics systems under supply and demand uncertainty, Expert Syst. Appl. 42 (15-16) (2015) 6237–6254.
[7] F. Li, G. Sun, X. Huang, J. Rong, Q. Li, Multiobjective robust optimization for crashworthiness design of foam filled thin-walled structures with random and interval uncertainties, Eng. Struct. 88 (2015) 111–124.
[8] I. Chakraborty, V. Kumar, S.B. Nair, R. Tiwari, Rolling element bearing design through genetic algorithms, Eng. Optim. 35 (6) (2003) 649–659.
[9] B.R. Rao, R. Tiwari, Optimum design of rolling element bearings using genetic algorithms, Mech. Mach. Theory 42 (2) (2007) 233–250.
[10] R. Tiwari, S. Gupta, Multi-objective design optimisation of rolling bearings using genetic algorithms, Mech. Mach. Theory 42 (10) (2007) 1418–1443.
[11] L. Tudose, G. Kulcsar, C. Stănescu, Pareto approach in multi-objective optimal design of single-row cylindrical rolling bearings, in: G. Dobre (Ed.), Power Transmissions, Vol. 13 of Mechanisms and Machine Science, Springer Netherlands 2013, pp. 519–528.
[12] H. Sjoväll, Belastningsfördelningen inom kul-och rull-lager vid givna yttre radial-och axialbelastningar (The load distribution within ball and roller bearings under given external radial and axial load), Teknisk Tidskrift, Mek 9.
[13] A.B. Jones, Analysis of Stresses and Deflections, Technical Report NREL/TP-500-36881, vol. 1 and 2New Departure Division, General Motors Corp., Bristol, Connecticut, 1946.
[14] A.B. Jones, A general theory for elastically constrained ball and radial roller bearings under arbitrary load and speed conditions, J. Fluids Eng. 82 (2) (1960) 309–320.
[15] J.M. De Mul, J. Vree, D. Maas, Equilibrium and associated load distribution in ball and roller bearings loaded in five degrees of freedom while neglecting friction — part I: general theory and application to ball bearings, J. Tribol. 111 (1) (1989) 142–148.
[16] J.M. De Mul, J. Vree, D. Maas, Equilibrium and associated load distribution in ball and roller bearings loaded in five degrees of freedom while neglecting friction — part II: application to roller bearings and experimental verification, J. Tribol. 111 (1) (1989) 149–155.
[17] T. Lim, R. Singh, Vibration transmission through rolling element bearings, part I: bearing stiffness formulation, J. Sound Vib. 139 (2) (1990) 179–199.
[18] R. Singh, T.C. Lim, Vibration Transmission Through Rolling Element Bearings in Geared Rotor System, Final Report — Part I RF Project 765863/719176, The Ohio State University, Grant No. NAG 3-773, December 1989.
[19] A. Gunduz, Multi-Dimensional Stiffness Characteristics of Double row Angular Ball Bearings and Their Role in Influencing Vibration Modes(PhD Thesis) The Ohio State University, Columbus, Ohio, 2012.
[20] L. Houpert, A uniform analytical approach for ball and roller bearings calculations, J. Tribol. 119 (4) (1997) 851–858.
[21] L. Houpert, An enhanced study of the load–displacement relationships for rolling element bearings, J. Tribol. 136 (1) (2014) 1–11 (011105).
[22] X. Hernot, M. Sartor, J. Guillot, Calculation of the stiffness matrix of angular contact ball bearings by using the analytical approach, J. Mech. Des. 122 (1) (2000) 83–90.
[23] N.T. Liao, J.F. Lin, A new method for the analysis of deformation and load in a ball bearing with variable contact angle, J. Mech. Des. 123 (2) (2001) 304–312.
[24] N.T. Liao, J.F. Lin, Ball bearing skidding under radial and axial loads, Mech. Mach. Theory 37 (1) (2002) 91–113.
[25] C. Bai, Q. Xu, Dynamic model of ball bearings with internal clearance and waviness, J. Sound Vib. 294 (1–2) (2006) 23–48.
[26] T.A. Harris, M.N. Kotzalas, Rolling Bearing Analysis: Essential Concepts of Bearing Technology, Taylor & Francis/CRC Press, 2007.
[27] T.A. Harris, M.N. Kotzalas, Rolling Bearing Analysis: Advanced Concepts of Bearing Technology, Taylor & Francis/CRC Press, 2007.
[28] D. Noel, S. Le Loch, M. Ritou, B. Furet, Complete analytical expression of the stiffness matrix of angular contact ball bearings, J. Tribol. 135 (4) (2013) 1–8 (041101).
[29] Y. Guo, R.G. Parker, Stiffness matrix calculation of rolling element bearings using a finite element/contact mechanics model, Mech. Mach. Theory 51 (2012) 32–45.
[30] E.P. Gargiulo Jr., A simple way to estimate bearing stiffness, Mach. Des. 52 (1980) 107–110.
[31] D. Dentcheva, Optimization models with probabilistic constraints, in: G. Calafiore, F. Dabbene (Eds.), Probabilistic and Randomized Methods for Design under Uncertainty, Springer 2006, pp. 49–97.
[32] P. Brandimarte, Handbook in Monte Carlo Simulation: Applications in Financial Engineering, Risk Management, and Economics, Wiley Handbooks in Financial Engineering and Econometrics, Wiley, 2014.
[33] X.-S. Yang, S. Deb, Cuckoo Search via lévy flights, NaBIC, IEEE 2009, pp. 210–214.
[34] C. Brown, L. Liebovitch, R. Glendon, Lévy flights in dobe juhoansi foraging patterns, Hum. Ecol. 35 (1) (2007) 129–138.
[35] X.-S. Yang, Cuckoo Search and firefly algorithm: Overview and analysis, in: X.-S. Yang (Ed.), Cuckoo Search and Firefly Algorithm, Vol. 516 of Studies in Computational Intelligence, Springer International Publishing 2014, pp. 1–26.
[36] ISO 4406:1999(E) hydraulic fluid power — fluids — method for coding the level of contamination by solid particles, International Organization for Standardization (1999).
[37] ISO/TS 16281:2008(E) rolling bearings — methods for calculating the modified reference rating life for universally loaded bearings, International Organization for Standardization (2008).
[38] ISO 281:2007(E) rolling bearings — dynamic load ratings and rating life, International Organization for Standardization (2007).
[39] W.B. Powell, I.O. Ryzhov, Optimal Learning, Wiley Series in Probability and Statistics, J. Wiley, Hoboken (N.J.), 2012.
[40] F. Scholz, Tolerance stack analysis methods, Tech. Rep. (1995).
[41] T.H.G. Megson, Structural and Stress Analysis 2nd Edition, Elsevier, San Diego, CA, 2005.
[42] S. Creţu, I. Bercea, N. Mitu, A dynamic analysis of tapered roller bearing under fully flooded conditions part 1: theoretical formulation, Wear 188 (1–2) (1995) 1–10.